water

MDPI

Article

Site-Specific Hydrogeological Characterization for Radiological Safety: Integrating Groundwater Dynamics and Transport

Soo-Gin Kim [1,2], Hong-Il Kwon [1], Jeoung-Seok Yoon [3], Chan-Hong Kim [1,4], Hyo Heo [1] and Chung-Mo Lee [2,5,*]

[1] Safety Assessment Team, Korea Radioactive Waste Agency, Gyeongju 38062, Republic of Korea; point0410@korad.or.kr (S.-G.K.); hong1k@korad.or.kr (H.-I.K.); chahkim@korad.or.kr (C.-H.K.); hheo@korad.or.kr (H.H.)
[2] Department of Geological Sciences, Pusan National University, Busan 46241, Republic of Korea
[3] DynaFrax UG Ltd., 14473 Potsdam, Germany; js.yoon@dynafrax.com
[4] Korea Mine Rehabilitation and Mineral Resources Corporation (KOMIR), Wonju 26464, Republic of Korea
[5] Institute for Future Earth, Busan 46241, Republic of Korea
* Correspondence: chungmo@pusan.ac.kr

Abstract: The radiological impact of radionuclide transport via groundwater pathways at the Wolsong Low- and Intermediate-Level Waste (LILW) Disposal Center was estimated by considering site-specific characteristics, including hydrogeology, geochemistry, and land use. Human intrusion scenarios, such as groundwater well development, were analyzed to evaluate potential pumping volumes and radionuclide migration pathways. Particular attention was given to the hydrological and geochemical aspects of radionuclide transport, with a focus on local aquifer heterogeneity, flow dynamics, and interactions with engineered barriers and surrounding rock formations that delay radionuclide migration through sorption and other retention mechanisms. Sorption coefficients (K_d), calibrated using site-specific geochemical data, were incorporated to ensure realistic modeling of radionuclide behavior. A hierarchical approach integrating scenario screening, particle tracking techniques, and mass transfer modeling was employed. Numerical simulations using FEFLOW ver. 7.3 and GoldSim ver. 14.0 software provided insights into near-field and far-field transport phenomena under well pumping conditions. The results revealed distinct spatial flux behaviors, where carbon-14 (^{14}C) dominated near-field flux due to its high inventory, while technetium-99 (^{99}Tc) emerged as the primary dose contributor in the far-field flux, owing to its anionic nature and limited sorption capacity. Additionally, under high-pH conditions near concrete barriers, cellulose degradation into isosaccharinic acid was identified, enhancing radionuclide mobility through complex formation. These findings underscore the importance of site-specific sorption and speciation parameters in safety assessment and highlight the need for accurate geochemical modeling to optimize waste placement and ensure long-term disposal safety. The outcomes provide valuable insights for optimizing waste placement and contribute to the development of evidence-based safety strategies for long-term performance assessment.

Keywords: radioactive waste disposal; groundwater; radiological impact; site-specific safety assessment; radionuclide migration; human intrusion scenario; Wolsong LILW Disposal Center

check for updates

Academic Editor: Alexander Yakirevich

Received: 20 November 2024
Revised: 7 January 2025
Accepted: 8 January 2025
Published: 11 January 2025

Citation: Kim, S.-G.; Kwon, H.-I.; Yoon, J.-S.; Kim, C.-H.; Heo, H.; Lee, C.-M. Site-Specific Hydrogeological Characterization for Radiological Safety: Integrating Groundwater Dynamics and Transport. *Water* **2025**, *17*, 186. https://doi.org/10.3390/w17020186

Copyright: © 2025 by the authors. Licensee MDPI, Basel, Switzerland. This article is an open access article distributed under the terms and conditions of the Creative Commons Attribution (CC BY) license (https://creativecommons.org/licenses/by/4.0/).

1. Introduction

Nuclear energy serves as a low-carbon electricity source, playing a crucial role in mitigating climate change and enhancing energy security. Nuclear energy offers significant

advantages, including minimal greenhouse gas emissions compared to fossil fuels and the ability to provide reliable baseload electricity at scale [1,2]. However, the operation of nuclear power facilities inevitably generates radioactive waste as a by-product.

Since the Manhattan Project in 1942, various options for radioactive waste disposal have been extensively studied, including sub-seabed disposal, disposal in glaciated regions, extraterrestrial disposal, and deep geological disposal [3]. After decades of research, geological disposal has emerged as the most viable method for managing radioactive waste, effectively balancing technical feasibility with environmental protection [4,5]. This approach, first proposed by the National Academy of Sciences in 1957, relies on a multi-barrier system that integrates engineered barriers, such as waste containers and backfill materials, with natural barriers like host rock formations to prevent radionuclide migration into the biosphere [5,6].

Despite these advancements, selecting a suitable site for radioactive waste disposal remains a global challenge, often hindered by public acceptance, geological suitability, and long-term safety concerns. However, the Republic of Korea has made significant progress by successfully operating the Wolsong Low- and Intermediate-Level Waste (LILW) Disposal Center. To enhance efficiency, additional facilities are being developed sequentially based on waste classification, including underground silo-type, near-surface, and landfill-type facilities. The Wolsong site employs a multi-barrier system that combines engineered barriers with natural geological formations, ensuring long-term safety and environmental protection.

Groundwater interaction with the waste form plays a critical role in radionuclide transport within geological disposal facilities. Radionuclides mobilized by geochemical processes migrate through fractured rock aquifers, where heterogeneity significantly affects transport pathways. The heterogeneity of aquifers significantly influences migration pathways, necessitating site-specific assessments to ensure long-term safety [7,8]. Previous studies, such as Cheong et al. [9], have demonstrated that discrete fracture network (DFN) models, combined with well pumping analyses, provide critical insights into radionuclide migration under various hydrogeological conditions. This research builds on these findings to evaluate transport processes under diverse scenarios. Site-specific hydrogeological conditions, including fracture networks, hydraulic connectivity, and low-permeability zones, significantly influence transport behaviors. These factors not only influence flow and transport through fractures but also highlight the role of immobile water zones in delaying contaminant migration through diffusion-dominated mechanisms. Additionally, well pumping activities can modify local hydraulic gradients, flow directions, and transport behaviors, particularly in areas with strong aquifer heterogeneity.

A safety assessment of a disposal facility ensures that radiological impacts remain within regulatory limits by evaluating the performance of the multi-barrier system under both normal and unexpected conditions. These assessments integrate the combined performance of the waste form, engineered barriers, and site-specific environmental conditions, with a particular focus on groundwater flow and radionuclide migration [10,11]. Post-closure safety assessments are generally categorized into three scenarios: normal, abnormal probability, and human intrusion [10]. While the normal scenario considers gradual radionuclide migration under expected conditions, the human intrusion scenario evaluates the radiological consequences of inadvertent activities, such as groundwater well construction, that may occur after the post-closure management period ends [12]. In the Republic of Korea, such impacts must remain below the public dose limit of 1 mSv/year and be reduced to as low as reasonably achievable (ALARA) [13].

To address these concerns, future anthropogenic activities were predicted based on site characteristics and historical land use patterns. Through comparisons with international

cases and an initial screening of Features, Events, and Processes (FEPs) using the ISAM (Improvement of Safety Assessment Methodologies) reference list [14], scenarios such as seismic events, flooding, and mining activities were excluded. The analysis identified exploratory drilling activities—particularly those related to groundwater well construction—as the most significant human intrusion scenario due to their potential to alter groundwater flow and facilitate radionuclide transport [15].

To systematically evaluate radionuclide transport and radiological impacts under such scenarios, a hierarchical approach was adopted. This methodology integrates scenario screening, particle tracking techniques, and mass transfer modeling to assess potential exposure pathways. By systematically managing uncertainties and adopting conservative assumptions, the proposed framework offers a robust tool for evaluating long-term safety and ensuring compliance with regulatory standards. The following sections provide detailed explanations of each stage of the methodology, reinforcing the reliability of geological disposal systems in protecting human health and the environment.

2. Study Area

2.1. Site Overview

The Wolsong LILW Disposal Center (Figure 1), located near the southeastern coast of the Korean Peninsula, is the nation's only radioactive waste disposal facility.

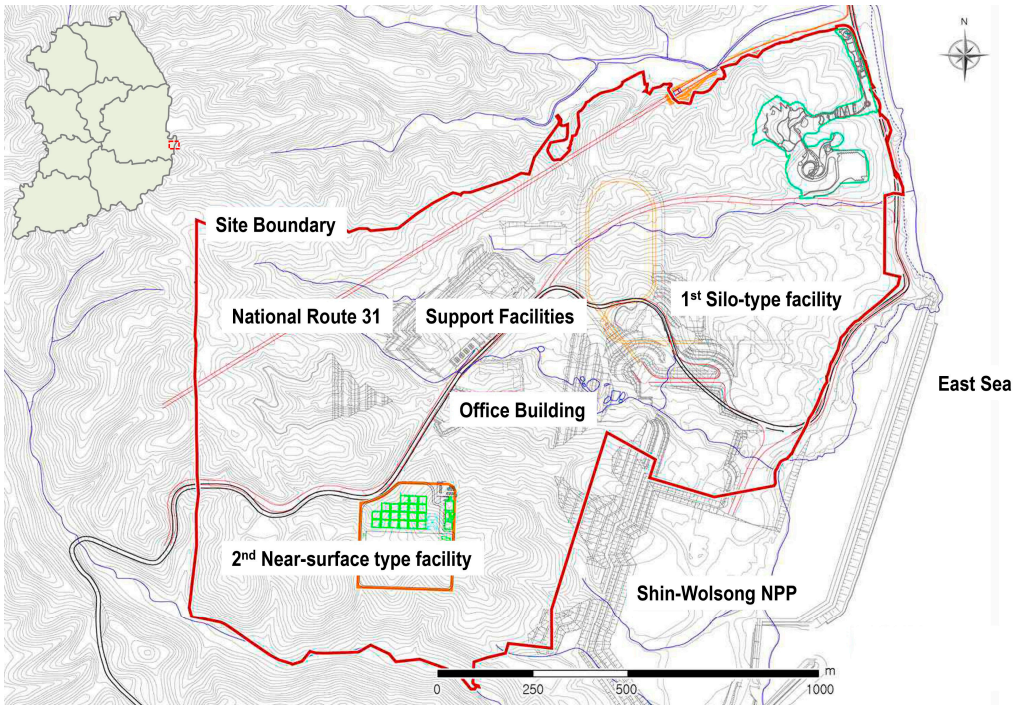


Figure 1. Map of study area (Southeastern of Korea).

The site covers a total area of approximately 2.05 million m^2, extending from mountainous terrain in the northwest to its eastern boundary adjacent to the East Sea. This results in a typical hilly landscape with a topographic orientation developing from northwest to southeast.

2.2. Topographic

Analysis of the topographic characteristics of the study area shows that a major ridge extends north–south along the western boundary of the site, with east–west ridges branching off to the east. Smaller spurs diverging from these ridges predominantly extend

in northeastern or southeastern directions. This topographic structure also influences the development of water systems, resulting in a general eastward flow tendency for most of them.

The study area, located within a minor mountain range, exhibits minimal surface water system development, leading to extremely limited surface water availability. Furthermore, the small watershed area precludes hydrological conditions that could induce large-scale flooding. In particular, the absence of rivers within the watershed effectively negates the potential for fluvial erosion or flooding.

As of 2005, residential settlements and transportation infrastructure were established along the central portion of the study area, while construction of a new nuclear power facility was in progress near the site's southeastern boundary (Figure 2).



Figure 2. Aerial photograph of the Wolsong LILW Disposal Center before development (courtesy of Google Earth, 2005).

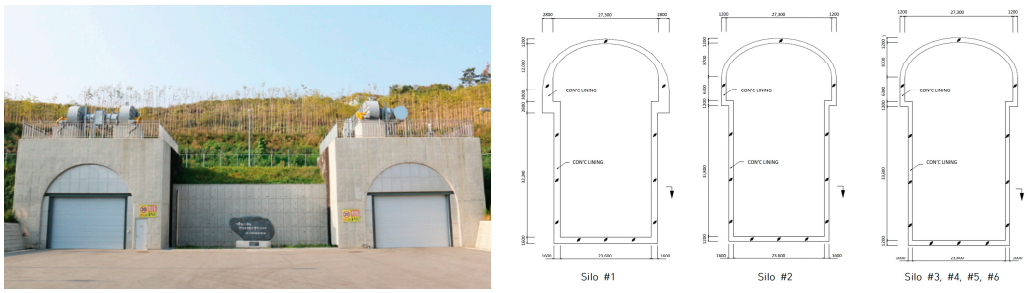
Following the construction of the disposal facility, significant topographic modifications occurred at the disposal site (Figure 3). Two spoil disposal areas, containing excavated material from the construction of Phase 1 silo-type disposal facility construction, were established adjacent to the surface support facilities. To accommodate additional excavated material generated during the mountain excavation for the Phase 2 near-surface disposal facility, one supplementary spoil disposal area was added to the existing sites, and six new disposal areas were constructed. During these development activities, the original water system that traversed the site's central area was permanently altered, with no possibility of restoration to its natural state following the closing of the disposal facilities. The green shaded areas in the eastern part of Figure 3 represent PWR (Pressurized Water Reactor) nuclear power facilities.



Figure 3. Aerial photograph of the Wolsong LILW Disposal Center after development (courtesy of Google Earth, 2023).

2.3. Target Dsposal Facility Characteristics

The Wolsong LILW Disposal Center consists of two sequential development phases at a single site: the silo-type (Phase 1) and the near-surface type (Phase 2) [16]. This assessment was conducted exclusively for the Phase 1 silo-type disposal facility. Each silo is a cylindrical concrete structure with a diameter of 23.6 m and a height of 50 m (Figure 4). The silos are constructed into bedrock at depths ranging from 80 to 130 m below sea level. The thickness of the concrete walls varies from 1.0 to 1.6 m, designed in accordance with the classification of the surrounding rock mass.



(**a**) (**b**)

Figure 4. Phase 1 silo-type facility at Wolsong LILW Disposal Center: (**a**) entrance view; (**b**) design layout of disposal silos.

2.4. Groundwater Level Distribution

The spatial distribution of groundwater levels within the site was characterized using data collected from 45 observation wells equipped with automated monitoring systems. These wells provided continuous water level measurements, ensuring a robust dataset for analysis. Geostatistical interpolation using the Kriging method was applied to quantitatively assess the spatial variability in groundwater levels across the site. Figure 5 shows the interpolated groundwater level distribution across the site.

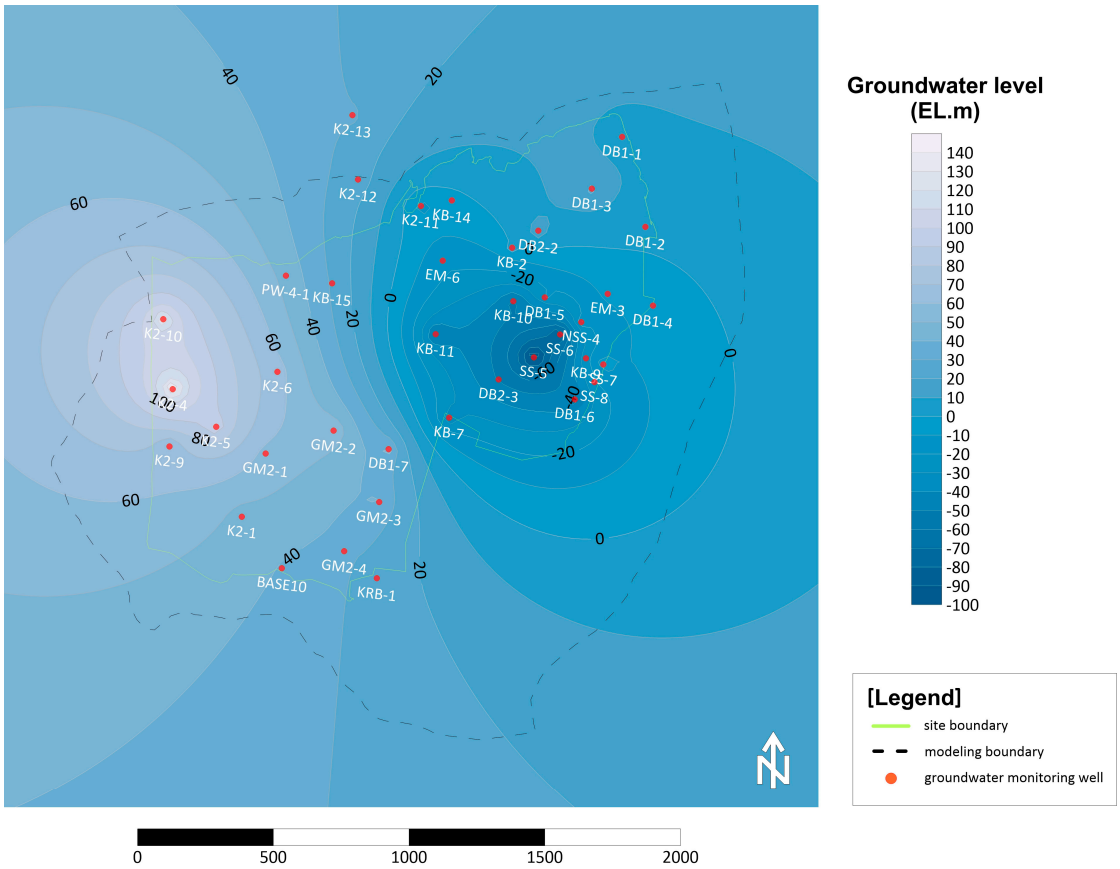


Figure 5. Groundwater level distribution at the Wolsong LILW Disposal Center site.

The groundwater flow model was initialized using stabilized groundwater levels measured in September 2018, following the operation of the Phase 1 silo-type disposal facility and the completion of site preparation activities for the Phase 2 near-surface disposal facility. Elevated groundwater levels are prominent near wells K2-4 and K2-10 along the western boundary, primarily attributed to the steep topographic gradient in this region, which enhances recharge and limits lateral flow. Conversely, the eastern portion of the site features a silo structure extending into the saturated zone at EL. -130 m. Around this silo, a significant groundwater drawdown zone is observed near wells SS-5 and SS-6. This drawdown is induced by the engineered drainage system designed to prevent groundwater contact with the silo during its operational phase.

2.5. Rock Mass Characteristics

The study area comprises crystalline rocks in the northwest and sedimentary rocks in the remaining regions, with several faults present throughout the site. The Phase 1 silo-type facility is located within the saturated crystalline rock zone, while the Phase 2 near-surface facility is positioned above the unsaturated sedimentary rock formation. Figure 6 illustrates the spatial distribution of hydraulic conductivity (Kxx) in the rock masses, derived from DFN modeling [9].

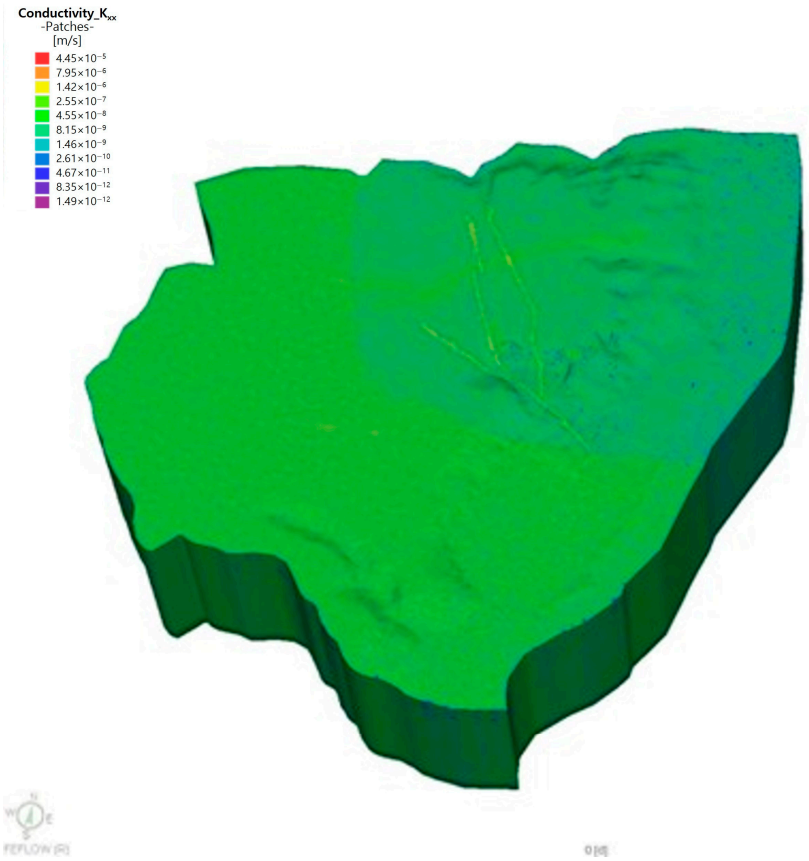


Figure 6. Spatial distribution of hydraulic conductivity (K_{xx}) derived from DFN modeling at the Wolsong LILW Disposal Center site.

Fault zones within the rock mass generally exhibit higher permeability than the surrounding matrix, acting as preferential pathways for groundwater flow. The contrast in permeability between sedimentary and crystalline rocks is particularly distinct, with sedimentary formations typically exhibiting greater permeability. These structural and lithological heterogeneities result in an anisotropic hydraulic conductivity distribution, significantly influencing groundwater flow directions and velocities. This variability plays a critical role in shaping solute transport patterns across the site.

2.6. Land Use

An analysis of land use by category within 10 km radius of the site revealed the following distribution, as shown in Table 1: forestland 71.6%, rice paddies 11.6%, fields 5.4%, orchards, pasture 0.1% and other 11.3% [17].

Table 1. Land use status within 10 km radius of the Wolsong LILW Disposal Center site.

Land Use Type	Fields	Paddies	Orchards	Pasture	Forestland	Other [1]
Area [ha]	849.1	1823.3	5.8	11.7	11,229.2	1776.2
Percentage [%]	5.41	11.62	0.04	0.07	71.55	11.32

Note: [1] In this context, "Other" includes various land types such as residential, industrial, educational, railway, and recreational areas, as well as embankments, reservoirs, parks, religious and historical sites, cemeteries, etc.

This land use pattern is characteristic of South Korea's topography, where forested areas account for approximately 63.4% of the total land area [18]. The high proportion of forested land in the study area reflects the general features of the Korean Peninsula, which is dominated by mountainous terrain and has limited arable land.

2.7. Climate

The Republic of Korea is situated in the mid-latitude temperate zone and experiences four distinct seasons [18,19]. Winter is characterized by cold and dry conditions due to the Siberian high-pressure system, while summer brings hot and humid weather under the influence of the North Pacific high-pressure system. Spring and autumn feature mild temperatures and clear weather. The annual average temperature ranges from 10 °C to 15 °C, with August being the warmest month (23 °C to 26 °C) and January the coldest (−6 °C to 3 °C). The study area receives an annual precipitation of 1000 mm to 1300 mm, with approximately 50% to 60% of this total occurring during the summer months.

The World Meteorological Organization (WMO) defines standard climate normal as 30-year averages of meteorological conditions, with updates recommended every decade [20]. An analysis of 30-year (1985–2014) meteorological data from the Ulsan weather station, located near the study area, reveals an annual mean temperature of approximately 14.6 °C and annual precipitation of about 1286.8 mm (Figure 7).

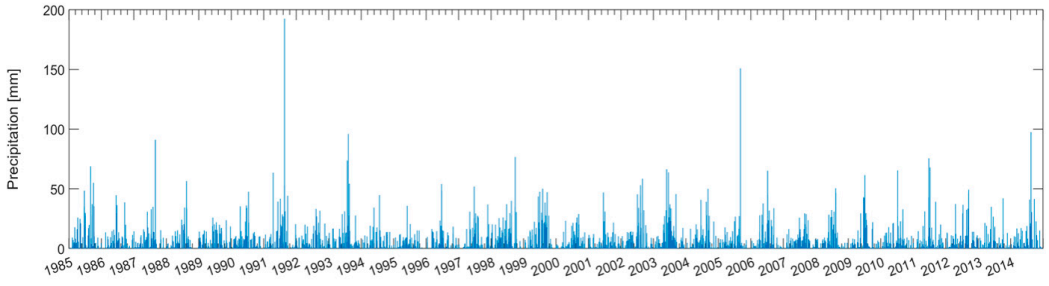


Figure 7. The 30-year climate normal (1985–2014) for the Ulsan weather station.

2.8. Population

Within a 10 km radius of the study area, there are five administrative districts. A baseline demographic survey reported a total resident population of 17,050, with an average population density of 99.6 persons/km^2 [21]. Notably, the administrative district containing the disposal facility has a population density of 38.0 persons/km^2, which is approximately 2.6 times lower than the average within the 10 km radius. This relatively low density is attributed to the site's peripheral location, far from urban centers.

According to the Environmental Impact Assessment (EIA) report for the disposal facility site, the development of the facility led to the relocation of 52 households within the site boundary, displacing approximately 156 residents based on an average household size of three persons [22].

2.9. Status of Groundwater Wells

Following the development of the disposal facility, all pre-existing domestic and agricultural wells within the study area were decommissioned. Currently, multiple monitoring wells are in operation across the site to track groundwater characteristics and potential radionuclide releases as part of the environmental monitoring program.

Historical records show that there were 13 domestic-use wells and one agricultural-use well within the site boundary. The capacity (pumping rate) of the domestic wells ranged from 3600 to 24,000 m^3/year, with 10 out of the 13 wells (77%) drilled to a depth of 100 m (Table 2).

Table 2. Specifications and characteristics of pre-existing wells within the site boundary.

Location	ID	Usage	Potable	Capacity [m^3/year]	Depth [m]	Diameter [m]
	A	Domestic	Yes	3600	100	0.15
	B	Domestic	Yes	3500	90	0.20
	C	Domestic	Yes	-	100	0.15
	D	Domestic	No	-	100	0.15
	E	Domestic	Yes	24,000	100	0.15
	F	Domestic	Yes	9000	100	0.15
	G	Domestic	Yes	-	100	0.15
	H	Domestic	No	3600	35	0.10
	I	Domestic	No	-	100	0.15
	J	Domestic	No	-	100	0.15
	K	Domestic	No	-	100	0.20
	L	Domestic	Yes	17,500	60	0.15
	M	Domestic	Yes	18,000	100	0.20
	N	Agricultural	No	50,000	50	0.15

Note: Wells highlighted in gray were located within the site boundary.

The largest capacity well on the site was the agricultural well located in the center of the site. It had a developed depth of 50 m, a pumping rate of 50,000 m^3/year, and a diameter of 0.15 m, similar to that of domestic wells. Given the distribution of agricultural land and wells within the disposal site, it is reasonable to assume that agricultural water needs were primarily met through surface water and rainfall. The well development pattern suggests that wells were constructed and utilized at higher elevations where securing sufficient water quantities was more challenging, aligning with typical well development practices.

2.10. Geochemical Environment Around the Silo

The engineered barrier system of the Phase 1 silo-type disposal facility consists of concrete walls with thicknesses ranging from 1.0 to 1.6 m, along with supplementary structures surrounding the silos. It is designed to delay the release of radionuclides into the biosphere. The hydration reaction between cement and water produces substantial amounts of calcium hydroxide ($Ca(OH)^2$), creating a highly alkaline environment with a pH of approximately 13. This high alkalinity extends to the surrounding structures of the silos, contributing to the overall chemical stability of the disposal system.

3. Methods

This study adopts a hierarchical approach integrating scenario screening, particle tracking techniques, and simplified mass transfer modeling to evaluate the long-term safety of radioactive waste disposal facilities.

As illustrated in Figure 8, the methodological framework outlines the stepwise approach used for the safety assessment of human intrusion scenarios. The process begins with the scenario screening phase, where site-specific topographical features and land use conditions are thoroughly analyzed to identify zones with a high probability of well development and assess potential exposure pathways for radioactive nuclides. This process is related to Section 4.1.

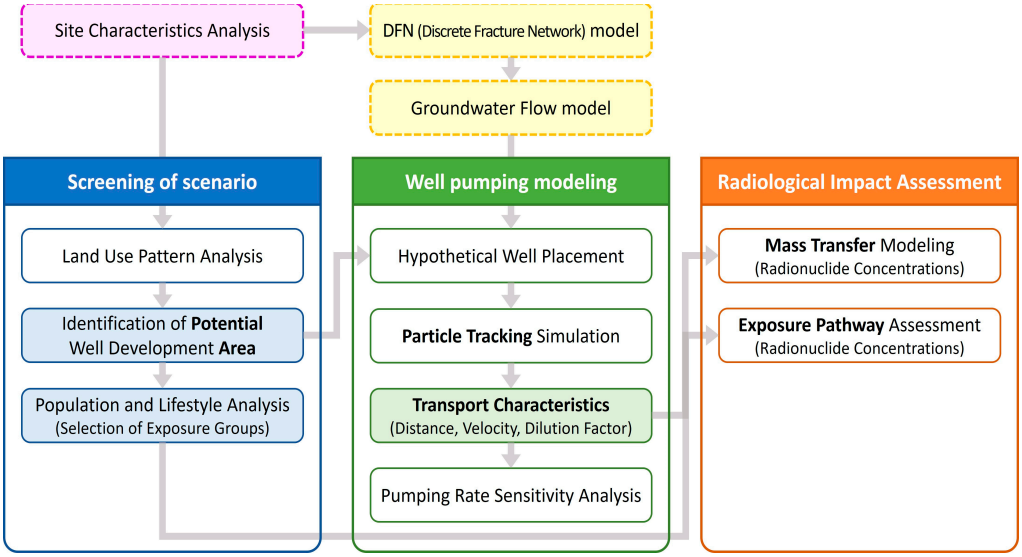


Figure 8. Methodological framework for the safety assessment of human intrusion scenarios.

A discrete fracture network (DFN)-based groundwater flow model, previously developed using FEFLOW ver. 7.3 software, incorporates stochastic representations of rock fractures to account for hydrogeological anisotropy [9]. Such representation is crucial as groundwater flow and contaminant transport in heterogeneous aquifers, influenced by both hydrogeological anisotropy and variations in hydraulic conductivity, exhibit complex behaviors that significantly influence radionuclide migration patterns [23]. Particle tracking techniques were applied to this model to quantitatively evaluate groundwater flow characteristics, extracting key parameters such as well inflow ratios (dilution factors), radionuclide transport distances, and velocities under well pumping scenarios. This process is related to Sections 4.2 and 4.3.

The extracted parameters served as essential input data for a mass transfer model, which simulates radionuclide transport from waste through engineered barriers and natural rock formations to the biosphere under simplified assumptions. The mass transfer model calculates nuclide-specific concentrations at biosphere release points, such as seas, wells, or other entry points into the ecosystem. These concentrations are then used to estimate expected radiation doses based on exposure pathways, including ingestion, inhalation, and external exposure. This process is detailed in Section 4.4.

This hierarchical approach offers a comprehensive assessment of radionuclide transport pathways and exposure mechanisms, facilitating the evaluation of long-term safety and ensuring compliance with regulatory requirements. By systematically managing uncertainties through conservative assumptions at each stage, the reliability of the results is further enhanced. The following sections provide detailed descriptions of each step in the assessment methodology.

3.1. Methods for Screening of Scenario

To evaluate the radiological impact of radionuclides released from disposal facilities, it is essential to establish appropriate scenarios. A "scenario" represents an assumed set of conditions used in safety assessments to estimate radionuclide release, transport, and subsequent radiological consequences. This study focused on developing scenarios to assess the radiological impact of inadvertent human intrusion, specifically where an intruder, unaware of the disposal facility's existence, installs and operates a power-driven well along groundwater pathways that may be contaminated by radionuclides from the disposed waste.

By analyzing current site characteristics and historical land use patterns, specific zones suitable for groundwater well development were identified within the study area. Based on existing patterns of human activity in the region, potential future groundwater utilization activities at the site were identified. These activities primarily include agriculture, livestock farming, and tourism, which are major consumers of groundwater in such areas.

3.2. Methods for Well Pumping Modeling

When radioactive waste interacts with infiltrating water within a disposal vault, radionuclides can be released into the environment in multiple phases, including gas and liquid. However, for conservative assessment purposes, it is assumed that all radionuclides dissolved from the waste through contact with infiltrating water are fully released and transported along groundwater pathways to environmental discharge points. When a well pumps groundwater along the contaminated flow path, a portion of the radionuclides enters the well, while the remainder is discharged and diluted in the sea. The well scenario evaluates the radiological impact on a representative individual resulting from the use of contaminated groundwater extracted through pumping.

The annual dose for the well scenario is given by:

$$E = \sum_i C_i \times DCF_i \times DF \quad (1)$$

where

- E: Annual effective dose [Sv/year],
- C_i: Flux of radionuclide i [Bq/year],
- DCF_i: Dose conversion factor for radionuclide i [Sv/Bq], and
- DF: Dilution factor [-].

In this study, the "dilution factor" represents the proportion of radionuclides released from the disposal facility that enter the well. To calculate this, a forward particle tracking method was employed, effectively analyzing contaminant and fluid behavior in complex flow fields. This methodology involved introducing a hypothetical multi-screen well into a steady-state groundwater flow model representing post-closure conditions of the disposal facility. By releasing multiple virtual particles from the source and tracking their trajectories, the proportion of contaminants entering the well could calculated, thus deriving the dilution factor (Figure 9).

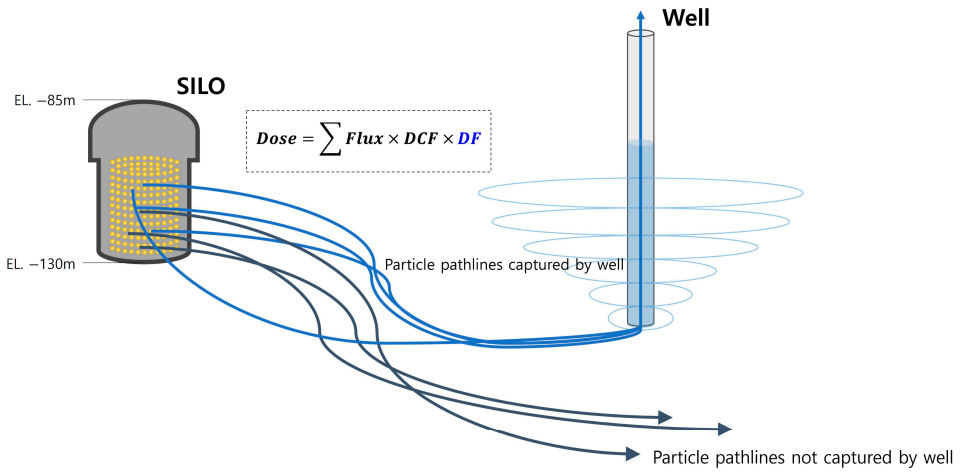


Figure 9. Conceptual model for predicting dilution factors in well scenarios.

The contaminant inflow ratio against the well is calculated using the following equation:

$$R_{inflow} = \frac{M_{well}}{M_{total}} \quad (2)$$

where

- R_{inflow}: Proportion of particles reaching the well, DF [-];
- M_{well}: Number of particles entering the well [nos.];
- M_{total}: Total number of released particles [nos.].

To identify the optimal location for a representative well, multiple hypothetical wells were positioned within the potential well development zones identified during scenario screening. Each hypothetical well location was evaluated based on the three key parameters below.

1. Contaminant inflow ratio: Fraction of contaminants entering the well.
2. Distance: Mean distance contaminants travel through groundwater to the well.
3. Velocity: Speed of groundwater, carrying contaminants, moving toward the well.

The selection criteria prioritized representative wells with:

- Higher contaminant inflow ratios,
- Shorter average contaminant traveling distances, and
- Faster average groundwater velocities.

This hierarchical approach ensured the identification of a well location that maximizes contaminant capture, thereby enabling a conservative evaluation for radiological impact assessments. The modeling and analysis were performed using FEFLOW, a finite element subsurface flow and transport simulation system developed by DHI.

3.3. Radiological Impact Assessment

Figure 10 illustrates the conceptual model of radionuclide migration within a Phase 1 silo-type disposal facility. It outlines the transport sequence, starting with the release of radionuclides from the waste form, moving through engineered barriers (e.g., backfill materials and concrete structures), entering the saturated zone, and ultimately reaching the biosphere. While the illustration appears two-dimensional for clarity, the study uses a one-dimensional (1D) model for computational efficiency and accurate representation of processes.

Once groundwater infiltrates the silo, it interacts with the radioactive waste, triggering physicochemical reactions that release radionuclides into the system. These radionuclides migrate primarily through diffusion across the concrete barriers into the surrounding natural rock, where diffusion dominates in low-permeability media like concrete.

Within the natural rock, radionuclide transport is governed by advection and dispersion mechanisms, which facilitate their migration through the porous medium. However, in both the near-field (around concrete barriers) and the far-field (natural rock), radionuclide transport is influenced by sorption interactions. In the near-field, radionuclides are partially retained through sorption onto the surfaces of concrete barriers, serving as an additional retention mechanism that delays their release into the surrounding environment. In the far-field, sorption onto mineral surfaces within natural rock further reduces radionuclide mobility, with retention efficiency depending on site-specific geochemical conditions, including pH, ionic strength, and mineral composition.

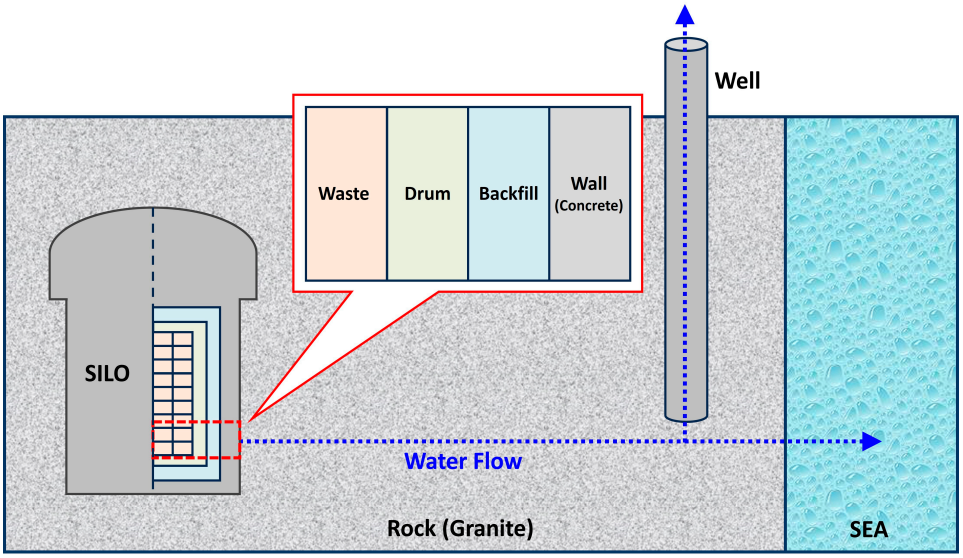


Figure 10. Conceptual model of radionuclide migration in Phase 1 silo-type disposal facility.

These sorption processes are incorporated into the modeling framework using sorption coefficients (K_d), calibrated to reflect the site-specific conditions accurately. The governing equation for radionuclide migration in porous media is as follows:

$$R\frac{\partial c}{\partial t} = D\frac{\partial^2 c}{\partial x^2} - v\frac{\partial c}{\partial x} - \lambda c \tag{3}$$

where R, retardation factor [-], is calculated as:

$$R = 1 + \frac{\rho_b \cdot K_d}{\theta} \tag{4}$$

where

- ρ_b: Bulk density of porous medium [M/L^3],
- K_d: Distribution coefficient [M/L^3],
- θ: Porosity of the medium [-],
- D: Dispersion coefficient [L^2/T],
- c: Radionuclide concentration in the porous medium [M/L^3],
- x: Distance of migration [L],
- v: Groundwater flow velocity [L/T], and
- λ: Radionuclide decay constant [T^{-1}].

Radionuclides that migrate through the natural rock eventually enter the local aquifer system (saturated zone) and may reach the biosphere. In this stage, the radionuclide concentration within the well compartment is determined by the radionuclide inflow rate (F) and the pumping rate (Q_w) according to the following equation:

$$C_w = \frac{F}{Q_w} \tag{5}$$

where

- C_w: Radionuclide concentration in the well [Bq/m^3],
- F: Radionuclide inflow rate to the well [Bq/year], and
- Q_w: Pumping rate [m^3/year].

In the near-field region, radionuclide migration is dominated by diffusion within concrete barriers and advection-dispersion processes in the surrounding natural rock. GoldSim

utilizes the Cell Pathway approach, which applies ordinary differential equation to simulate time-dependent changes in radionuclide concentrations. This approach is particularly suitable for modeling diffusion-dominated behavior in low-permeability regions.

The radionuclide mass balance in a specific cell is expressed as:

$$\frac{dM_s}{dt} = \sum_{k=1}^{n}(J_{in,k} - J_{out,k}) + S_s(t) \tag{6}$$

where

- M_s: Mass of radionuclide sss in the cell [M],
- $J_{in,k}$, $J_{out,k}$: Inflow and outflow rates to/from the cell [M/T], and
- $S_s(t)$: External source term for radionuclide s [M/T].

The diffusive flux between adjacent cells is defined as:

$$J_{diff} = G_{diff} \cdot (c_i - c_j) \tag{7}$$

where G_{diff}, the diffusive conductance, is calculated as:

$$G_{diff} = \frac{A}{\tau(L_i + L_j)} \tag{8}$$

where

- A: Cross-sectional area of the diffusive pathway [L^2],
- τ: Tortuosity factor [-], and
- L_i, L_j: Diffusion lengths for compartments i and j [L].

In the far-field region, advection is the dominant transport mechanism. GoldSim employs the Pipe Pathway approach, which uses partial differential equations to simulate radionuclide concentrations as a function of space and time.

The flux leaving the pathway is represented as:

$$J_{adv} = Q \cdot c \tag{9}$$

where

- Q: Volumetric flow rate [L^3/T].

Using the calculated radionuclide concentrations, GoldSim evaluates radiological doses from various exposure pathways, including ingestion, inhalation, and external exposure. The ingestion dose is calculated as:

$$D_{ing} = DCF_{ing} \cdot ING \cdot C_{ing} \tag{10}$$

where

- D_{ing}: Dose from ingestion [Sv/year],
- DCF_{ing}: Dose conversion factor for ingestion [Sv/Bq],
- ING: Annual ingestion rate [kg/year], and
- C_{ing}: Radionuclide concentration in ingested material [Bq/kg].

Radionuclide concentration in ingested material C_{ing} is calculated as:

$$C_{ing} = \frac{(CF_{crop} + (1 - F_{crop})S_{crop})C_{soil} + \mu_{crop}(d_{crop}C_{rw})}{(1 - \theta_{soil})\rho_{soil}} \tag{11}$$

where

- CF_{crop}: Concentration factor for radionuclide uptake by crops from soil [-],
- F_{crop}: Fraction of the crop grown on contaminated soil [-],
- S_{crop}: Source term for radionuclide input from irrigation or fallout [-],
- C_{soil}: Radionuclide concentration in soil [Bq/kg],
- μ_{crop}: Crop-specific radionuclide uptake efficiency factor [-],
- d_{crop}: Depth of soil layer influencing root uptake [m],
- C_{rw}: Radionuclide concentration in irrigation water [Bq/m^3],
- θ_{soil}: Soil porosity [-], and
- ρ_{soil}: Bulk density of soil [kg/m^3].

For consumption of sediment, the dose is calculated as:

$$D_{sed} = ING_{sed} \cdot D_{ing} \cdot \frac{c_{sed}}{(1-\theta_{sed})\rho_{gsed} + \theta_{sedu} \cdot \rho_w} \quad (12)$$

where

- D_{sed}: Radiological dose from sediment consumption [Sv/year],
- ING_{sed}: Sediment ingestion rate [kg/year],
- D_{ing}: Dose conversion factor for ingestion [Sv/Bq],
- c_{sed}: Radionuclide concentration in sediment [Bq/m^3],
- θ_{sed}: Porosity of the sediment [-],
- ρ_{gsed}: Grain density of sediment [kg/m^3],
- θ_{sedu}: Saturated porosity of sediment [-], and
- ρ_w: Density of water [kg/m^3].

For inhalation, the dose is calculated as:

$$D_{inh} = DCF_{inh} \cdot BR_{comp} \cdot O_{comp} \cdot C_{inh} \quad (13)$$

where

- D_{inh}: Radiological dose from inhalation [Sv/year],
- DCF_{inh}: Dose conversion factor for inhalation [Sv/Bq],
- BR_{comp}: Breathing rate [m^3/h],
- O_{comp}: Occupancy time [h/year], and
- C_{inh}: Radionuclide concentration in inhaled air [Bq/m^3].

For inhalation of dust, the dose is calculated as:

$$D_{dust} = D_{inh} \cdot BR_{sed} \cdot O_{sed} \cdot C_{air} \quad (14)$$

where

- D_{dust}: Radiological dose from inhalation of dust [Sv/year],
- BR_{sed}: Sediment inhalation rate [m^3/h],
- O_{sed}: Sediment exposure occupancy time [h/year], and
- C_{air}: Radionuclide concentration in airborne particles [Bq/m^3].

The radionuclide concentration in airborne particles is calculated as:

$$C_{air} = \frac{C_{sed} \cdot (R_{sed} - 1) \cdot dust_{sed}}{(1-\theta_{sed}) \cdot \rho_{gsed} \cdot R_{sed}} \quad (15)$$

where

- C_{sed}: Radionuclide concentration in sediment [Bq/m^3],
- R_{sed}: Resuspension factor of sediment [-], and

- $dust_{sed}$: Dust level above sediment surface [kg/m^3].

For external exposure, the dose is calculated as:

$$D_{ext} = DCF_{ext} \cdot O_{comp} \cdot C_{ext} \quad (16)$$

where

- D_{ext}: Radiological dose from external exposure [Sv/year],
- DCF_{ext}: Dose conversion factor for external exposure [(Sv/hr)/(Bq·m^3)], and
- C_{ext}: Radionuclide concentration in external media [Bq/m^3].

4. Results

4.1. Screening of Scenario

4.1.1. Scenario Overview

The International Commission on Radiological Protection (ICRP) classifies exposure scenarios into two categories: "natural processes", which are events expected to occur over decades, and "human intrusion", which are low-probability artificial events [24].

In the context of radioactive waste disposal, "natural scenarios" involve human activities that do not compromise the safety of the disposal system, while "human intrusion scenarios" focus on rare events that could disrupt its safety functions.

As part of the assessment for natural scenarios, groundwater utilization through natural springs and manually operated wells was analyzed. However, geological evaluations and groundwater flow modeling indicated negligible radionuclide transport to such wells. Additionally, the modeling confirmed that existing pumping wells would not disturb steady-state groundwater flow patterns. As a result, groundwater development and utilization activities were excluded from further assessment as part of normal scenarios.

4.1.2. Identification of Potential Areas for Groundwater Well Development

The presence of bedrock outcrops significantly influences the local hydrological cycle and soil erosion processes. These changes could substantially affect groundwater recharge and flow patterns, which are critical consideration for the development of groundwater wells.

Based on historical land use patterns and general land utilization trends, leveled areas, including cut slopes, are expected to be developed for residential or commercial purposes. Conversely, sections that retain their original topography may be utilized for agricultural activities. If wells are developed along or adjacent to groundwater flow paths that have been in contact with radioactive waste in the disposal facility, radiological exposure could occur through the use of contaminated groundwater. Among the four areas identified for future human activities, three sections (Section #1, Section #2, and Section #3) were determined to be potentially affected by groundwater passing through the Phase 1 silo-type disposal facility (Figure 11).

Section #3, a dredged area created during wharf construction near the coastline, was excluded from potential future use areas due to the high probability of seawater intrusion effects (Figure 12). This decision is supported by established research indicating that groundwater development in low-lying coastal areas can exacerbate seawater intrusion by reducing terrestrial groundwater flow and altering the freshwater-seawater interface [25]. The combination of coastal proximity and modified hydrogeological conditions makes this area unsuitable for future groundwater development.

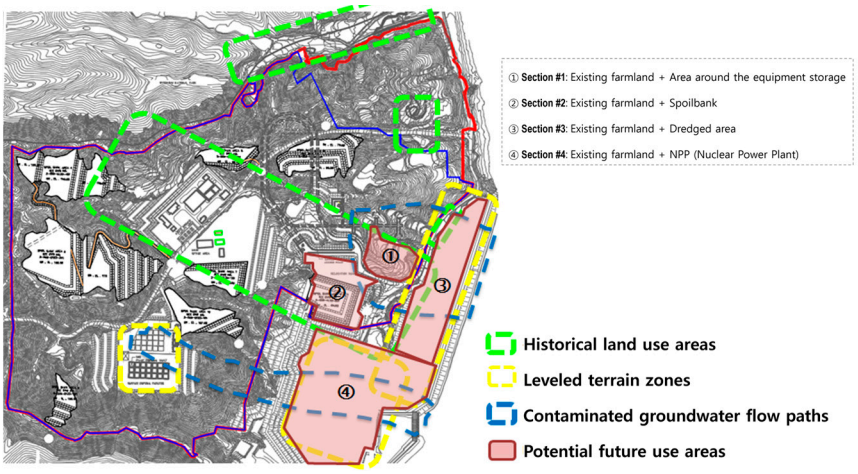
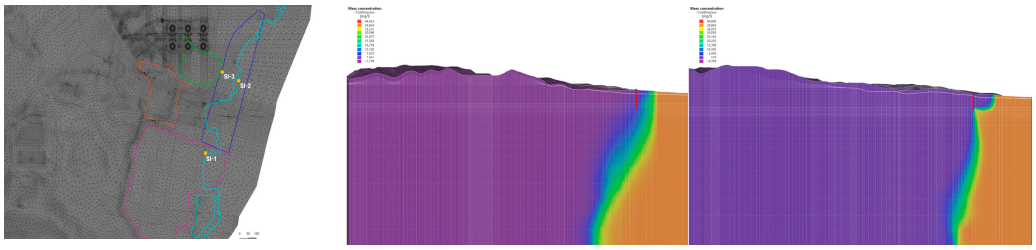


Figure 11. Identification of potential well development zones.



(**a**) (**b**) (**c**)

Figure 12. Evaluation of seawater intrusion impact in Section #3: (**a**) locations of monitoring wells for assessing seawater intrusion impact; (**b**) modeling results at hypothetical well SI-1; (**c**) modeling results at hypothetical well SI-3.

4.1.3. Evaluation of Future Groundwater Well Feasibility

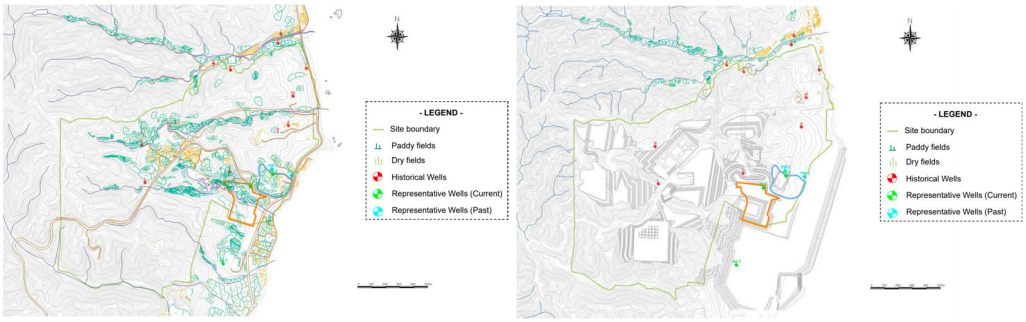
The site investigation revealed that residential zones were primarily located along the coastline and near major roads, while smaller settlements and agricultural lands were scattered inland, often following the paths of roads and streams (Figure 13a). Prior to site development, the study area exhibited distinct land use patterns characterized by agricultural activities and scattered residential settlements. Small-scale dry-field farming was concentrated in the gently sloping central area around clustered farmhouses, while paddy cultivation was practiced along developed watercourses. Two livestock barns were located near the site entrance. The groundwater utilization pattern reflected the area's water resource distribution:

- One agricultural well for rice farming in the central area,
- Two domestic wells near uphill residential areas,
- One well serving livestock barns, and
- Two wells supporting coastal commercial operations.

However, with the introduction of public water supply system well utilization has gradually declined throughout the region.

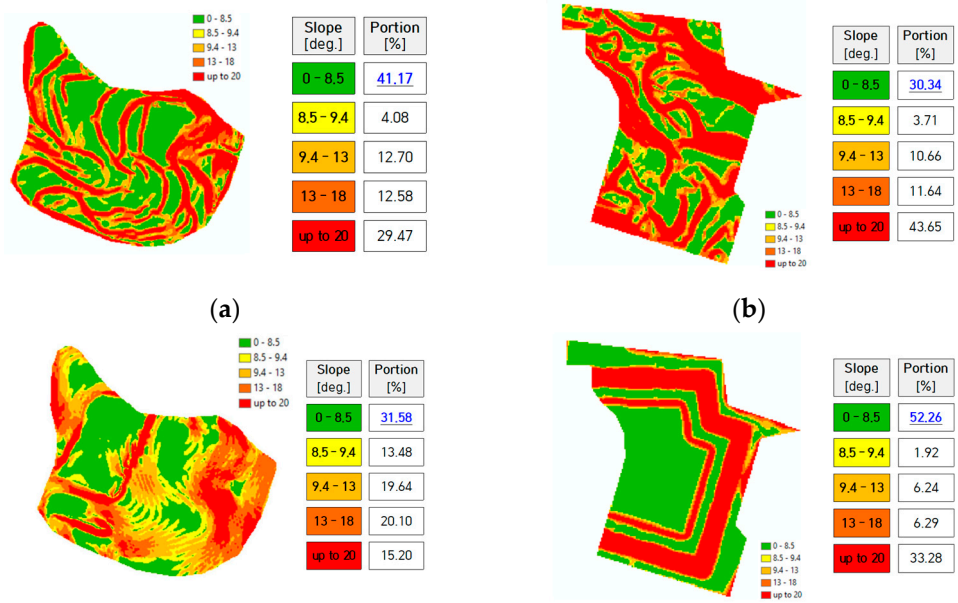
In contrast, the current disposal facility area is characterized by exposed bedrock outcrops and valleys filled with construction debris, resulting in a complete alteration of the original hydrological system (Figure 13b). The presence of bedrock outcrops significantly affects the local hydrological cycle and soil erosion processes throughout the site. These changes could have a substantial impact on groundwater recharge and flow patterns, which are critical considerations for the development of groundwater wells and the long-term safety assessment of the facility.

According to the Farmland Act of the Republic of Korea, land areas with an average slope of 15% or greater are considered to have unfavorable farming conditions and low agricultural productivity. Based on this criterion, areas with slopes less than 15% (approximately 8.5 degrees) within Sections #1 and Section #2—identified as potential well development zones—were analyzed. This slope threshold serves as a reference for assessing land suitability for agricultural activities and well installation (Figure 14).



(**a**) (**b**)

Figure 13. Land use status within the Wolsong LILW Disposal Center site: (**a**) digital topographic map before construction (2005); (**b**) digital topographic map after construction (2023).



(**a**) (**b**)

(**c**) (**d**)

Figure 14. Slope analysis results for potential future use areas. Numbers in blue font with underlines indicate slope ranges suitable for potential agricultural use: (**a**) topographic slope distribution of Section #1 before facility construction (2005); (**b**) topographic slope distribution of Section #2 before facility construction (2005); (**c**) topographic slope distribution of Section #1 after facility construction (2023); (**d**) topographic slope distribution of Section #2 after facility construction (2023).

Figure 14a,b present the pre-construction slope analysis of these areas, highlighting the topographic characteristics of the traditional terraced rice paddies that once existed in these regions. Areas with slopes less than 15%, considered suitable for agricultural activities and well development, comprised 15,516 m^2 (41.17%) and 14,809 m^2 (30.34%) of Sections #1 and #2, respectively. This classification is consistent with the Farmland Act of the Republic of Korea, which designates agricultural land with slopes exceeding 15% as disadvantaged farmland due to unfavorable farming conditions. Figure 14c,d present the post-construction slope analysis results. Areas with slopes less than 15% comprise 11,901

m^2 (31.58%) in Section #1 and 25,512 m^2 (52.26%) in Section #2. In Section #1, there was a reduction in areas with slopes below 15%, despite some leveling for equipment storage facilities, primarily due to the cessation of agricultural activities. In contrast, Section #2 showed an increase in flat terrain compared to pre-construction conditions, largely due to construction activities near the tunnel entrance.

Areas characterized by exposed bedrock are generally unsuitable for agricultural activities, particularly paddy farming. Although the study area is predominantly composed of exposed bedrock and disposal areas filled with construction debris, dry-field farming remains feasible in certain locations through specialized management practices, albeit with potentially reduced productivity. Consequently, for Sections #1 and #2, only dry-field farming was considered a viable agricultural scenario, while paddy farming was excluded from further assessment.

4.1.4. Classification of Potentially Exposed Groups

Various potential exposure groups were systematically evaluated based on projected land use patterns and site-specific characteristics. Tourist groups visiting recreational areas near the site and commercial facility operators in coastal areas were initially considered. Although these groups could be exposed through multiple pathways during beach activities, they were excluded from well-related exposure scenarios because coastal areas were deemed unsuitable for well development due to the risk of seawater intrusion.

The residential group, identified as potential future residents in the development areas, could be exposed to radiation through groundwater use for drinking and garden irrigation. Exposure scenarios for this group include internal exposure from consuming vegetables irrigated with potentially contaminated groundwater, and external exposure during gardening activities. However, demographic trends indicate a consistent population decline in surrounding areas, and the region's infrastructure plan suggests extensive expansion of public water supply systems. Given these socio-environmental changes, residential groundwater use scenarios were deemed unlikely and were therefore excluded from further assessment.

Two distinct farming groups were initially considered: the agricultural group engaged in large-scale farming activities and the agro-livestock group combining small-scale farming with livestock management. Both groups could be exposed through multiple pathways, including the consumption of contaminated crops, external exposure during farming activities, and, for the agro-livestock group, additional exposure through contaminated livestock products. As discussed in Section 4.1.3, the site characteristics make paddy farming impractical, and historically, livestock operations in this area were limited to a small number of barns. Nonetheless, this assessment conservatively selected an agro-livestock group—combining dry-field farming with small-scale livestock operations in Sections #1 and #2—as the representative exposure group.

4.2. Well Pumping Modeling

4.2.1. Assumptions and Scope of Analysis

The results of scenario screening identified Sections #1 and #2 as potential areas for groundwater well development. However, due to the practical limitations of drilling equipment accessibility on sloped terrain, the feasible well development area in Section #1 was limited to the leveled surface of the equipment storage facility site (Figure 15).

Representative well locations were determined through particle tracking modeling, which analyzed key parameters including particle influx ratios, groundwater travel distances and groundwater Darcy velocities.



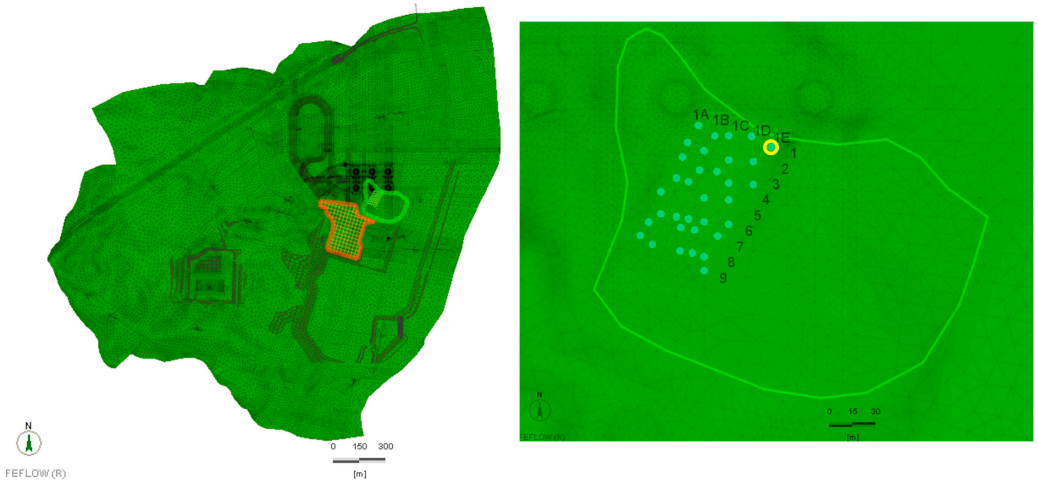
(**a**) (**b**)

Figure 15. Potential well development locations: (**a**) screening results (purple shaded areas); (**b**) aerial photograph of identified feasible areas.

4.2.2. Selection of Representative Well Location in Section #1

To identify locations with the highest potential radiological impact from radionuclides released from the silo in Section #1, multiple hypothetical wells were simulated (Figure 16). Each well was characterized with standardized specifications:

- Depth: 100 m below ground surface,
- Diameter: 15 cm, and
- Pumping rate: 25,000 m^3/year.



(**a**) (**b**)

Figure 16. Placement of hypothetical wells for site screening in Section #1. The dots within the area indicate virtual well installation points: (**a**) overview of well locations; (**b**) detailed view of well positions.

Particle tracking analysis of hypothetical wells indicated no particle influx from Silo #6. The highest particle influx was identified at location 1E-1 (highlighted by yellow circles in Figure 16b), where particles originating from Silo #5 exhibited the maximum influx rate of 14.3% among all candidate well locations (Table 3). The analysis revealed that Silo #1 and #3, located close to the wells and along the primary groundwater flow path, demonstrated significant particle inflow. In contrast, Silo #2 and #4, situated farther from the wells, exhibited notably lower particle capture rates. Silo #5, positioned against the groundwater flow direction, showed increased particle capture when pumping rates were higher or the distance to the wells was reduced.

Table 3. Particle influx ratios for hypothetical wells in Section #1.

Well	Particle Inflow Ratio (-)						
	SILO #1	**SILO #2**	**SILO #3**	**SILO #4**	**SILO #5**	**SILO #6**	**Mean**
1A-1	0.357	0.022	0.394	0.037	-	-	0.135
1B-1	0.252	0.032	0.074	0.424	-	-	0.130
1C-1	0.271	0.036	0.491	0.110	-	-	0.151
1D-1	0.180	0.008	0.350	0.146	0.032	-	0.119
1E-1	0.250	0.023	0.696	0.122	0.143	-	0.206
1A-2	0.439		0.397	-	-	-	0.139
1B-2	0.348		0.452	-	-	-	0.133
1C-2	0.283	0.032	0.475	-	-	-	0.132
1D-2	0.177	0.036	0.487	-	0.021	-	0.120
1A-3	0.339	-	0.305	-	-	-	0.107
1B-3	-	-	0.025	-	-	-	0.004
1C-3	0.113	-	0.408	-	-	-	0.087
1D-3	-	-	-	-	-	-	0.000
1E-3	-	-	-	-	-	-	0.000
1A-4	0.068	-	0.057	-	-	-	0.021
1C-4	0.107	-	0.122	-	-	-	0.038
1D-4	0.131	-	0.176	-	-	-	0.051
1A-5	0.236	-	0.024	-	-	-	0.043
1C-5	0.111	-	0.372	-	-	-	0.081
1D-5	0.120	-	0.270	-	-	-	0.065
1A-6	0.371	-	0.052	-	-	-	0.071
1B-6	-	-	-	-	-	-	0.000
1C-6	0.351	-	0.121	-	-	-	0.079
1D-6	0.353	-	0.322	-	-	-	0.113
1E-6	0.446	-	0.237	-	-	-	0.114
1A-7	0.214	-	-	-	-	-	0.036
1C-7	0.130	-	0.028	-	-	-	0.026
1D-7	0.235	-	0.050	-	-	-	0.048
1E-7	0.242	-	0.155	-	-	-	0.066
1A-8	0.121	-	-	-	-	-	0.020
1B-8	0.453	0.015	0.611	0.007	0.105	-	0.199
1C-8	0.117	-	0.018	-	-	-	0.023
1D-8	0.157	-	0.060	-	-	-	0.036
1E-9	0.175	-	0.043	-	-	-	0.036

The analysis of average contaminant transport distances during hypothetical well pumping revealed that location 1D-1 showed the shortest mean flow length of 222.4 m. At location 1E-1, the shortest flow path of 117.7 m was observed from Silo #5 (Table 4). The proximity of hypothetical wells to specific silos significantly affected particle transport distances, demonstrating the strong influence of well positioning on contaminant migration patterns. Particles from Silo #3 followed short paths (<100 m) due to the well's proximity, while particles from Silo #2 exhibited the longest migration distances. Interestingly, Silo #5, despite being positioned against the natural groundwater flow, displayed relatively short transport distances at certain well locations, highlighting the complex interplay between well location and groundwater dynamics.

Table 4. Mean contaminant transport distances during hypothetical well pumping in Section #1.

Well	Mean Transport Distances of Radionuclides (m)						
	SILO #1	**SILO #2**	**SILO #3**	**SILO #4**	**SILO #5**	**SILO #6**	**Mean**
1A-1	226.7	379.9	74.5	249.6	-	-	232.7
1B-1	249.8	352.9	108.0	275.2	-	-	246.5
1C-1	245.0	321.2	96.6	238.2	-	-	225.3
1D-1	275.7	312.6	135.8	248.7	139.0	-	222.4
1E-1	289.0	309.5	149.4	302.6	117.7	-	233.6

Analysis of mean Darcy velocities along groundwater flow paths during hypothetical well pumping revealed that location 1D-1 exhibited the highest average velocity of 6.41×10^{-9} m/s from all six silos (Table 5).

Table 5. Mean groundwater Darcy velocities during hypothetical well pumping in Section #1.

Well	Mean Groundwater Darcy Velocities (m/day)						
	SILO #1	**SILO #2**	**SILO #3**	**SILO #4**	**SILO #5**	**SILO #6**	**Mean**
1A-1	2.05×10^{-9}	5.65×10^{-9}	3.98×10^{-9}	3.15×10^{-9}	-	-	3.71×10^{-9}
1B-1	2.31×10^{-9}	7.35×10^{-9}	3.76×10^{-9}	1.95×10^{-9}	-	-	3.84×10^{-9}
1C-1	1.95×10^{-9}	1.03×10^{-8}	3.47×10^{-9}	2.01×10^{-9}	-	-	4.44×10^{-9}
1D-1	2.44×10^{-9}	1.69×10^{-8}	3.16×10^{-9}	2.08×10^{-9}	7.41×10^{-9}	-	6.41×10^{-9}
1E-1	2.20×10^{-9}	1.07×10^{-8}	3.44×10^{-9}	2.74×10^{-9}	6.37×10^{-9}	-	5.16×10^{-9}

The current inventory of radioactive waste shows an uneven distribution of cellulose-containing materials across silos, which could potentially enhance radionuclide mobility through the formation of isosaccharinic acid (ISA) [26]. As this heterogeneous distribution may significantly affect radiation exposure doses through sorption reduction effects, a detailed integrated analysis of groundwater flow characteristics and radiological impacts was conducted, considering the waste quantities disposed in each silo.

Dose assessment for hypothetical well pumping scenarios indicated that location 1E-1 showed the highest annual dose of 1.22×10^{0} mSv/year (Table 6). The elevated exposure was primarily attributed to cellulose-containing waste in Silo #5, where alkaline conditions promoted cellulose degradation to ISA, which enhanced radionuclide mobility, particularly niobium-94 (^{94}Nb).

Table 6. Total radiation doses during hypothetical well pumping in Section #1.

Category	1A-1	1B-1	1C-1	1D-1	1E-1
Total Dose [mSv/year]	6.21×10^{-2}	2.30×10^{-1}	7.85×10^{-2}	3.12×10^{-1}	1.22×10^{0}
Peak Time [year]	1798	1819	2078	2199	1778

The analysis of groundwater flow characteristics indicated that location 1E-1 showed the highest average contaminant influx rate via groundwater. Location 1D-1 had the shortest transport distance and the highest Darcy velocity; however, radiological assessment revealed that particle influx rates to wells (dilution factors) were more crucial than flow velocities or transport distances. Silo #5, containing substantial amounts of cellulose materials influencing radionuclide sorption, had the greatest impact on exposure doses at location 1E-1.

These results underscore that particle influx rates to wells and the quantity of disposed cellulose materials that affect radionuclide sorption are the primary determinants

of radiation doses. Consequently, location 1E-1 was selected as the representative well for Section #1.

4.2.3. Selection of Representative Well Location in Section #2

To determine areas with the highest potential radiological impact from radionuclides released from the silo in Section #2, multiple hypothetical wells were simulated (Figure 17). Each well was assigned standardized specifications:

- Depth: 100 m below ground surface,
- Diameter: 15 cm, and
- Pumping rate: 85,000 m^3/year.



(**a**) (**b**)

Figure 17. Placement of hypothetical wells for site screening in Section #2. The dots within the area indicate virtual well installation points: (**a**) overview of well locations; (**b**) detailed view of well positions.

Analysis of particle influx rates to hypothetical wells revealed that only particles released from Silo #1 entered the wells in Section #2, due to its location being separated from the main groundwater flow paths and showing opposite flow directions. At three locations (2I-1, 2J-1, and 2K-1) where particle influx rates were 100%, additional analyses of mean transport distances and Darcy velocities were conducted to determine the representative well location (Table 7).

Table 7. Particle influx ratios for hypothetical wells in Section #2.

Well	Particle Inflow Ratio (-)						
	SILO #1	SILO #2	SILO #3	SILO #4	SILO #5	SILO #6	Mean
2H-1	0.607	-	-	-	-	-	0.607
2I-1	1.000	-	-	-	-	-	1.000
2J-1	1.000	-	-	-	-	-	1.000
2K-1	1.000	-	-	-	-	-	1.000
2H-2	0.064	-	-	-	-	-	0.064
2I-2	0.333	-	-	-	-	-	0.333
2J-2	0.833	-	-	-	-	-	0.833
2K-2	0.868	-	-	-	-	-	0.868
2L-2	0.692	-	-	-	-	-	0.692
2M-2	0.936	-	-	-	-	-	0.936
2N-2	0.996	-	-	-	-	-	0.996
2O-2	0.996	-	-	-	-	-	0.996
2I-3	0.128	-	-	-	-	-	0.128
2J-3	0.261	-	-	-	-	-	0.261

Analysis of mean contaminant transport distances during hypothetical well pumping revealed that location 2J-1 showed the shortest average flow path length of 158.6 m from Silo #1 (Table 8).

Table 8. Mean contaminant transport distances during hypothetical well pumping in Section #2.

Well	Mean Transport Distances of Radionuclides (m)						
	SILO #1	SILO #2	SILO #3	SILO #4	SILO #5	SILO #6	Mean
2I-1	234.5	-	-	-	-	-	234.5
2J-1	158.6	-	-	-	-	-	158.6
2K-1	199.6	-	-	-	-	-	199.6

Analysis of mean Darcy velocities along groundwater flow paths during hypothetical well pumping showed that location 2J-1 exhibited the highest average velocity of 1.42×10^{-3} m/day from Silo #1 (Table 9).

Table 9. Mean groundwater Darcy velocities during hypothetical well pumping in Section #2.

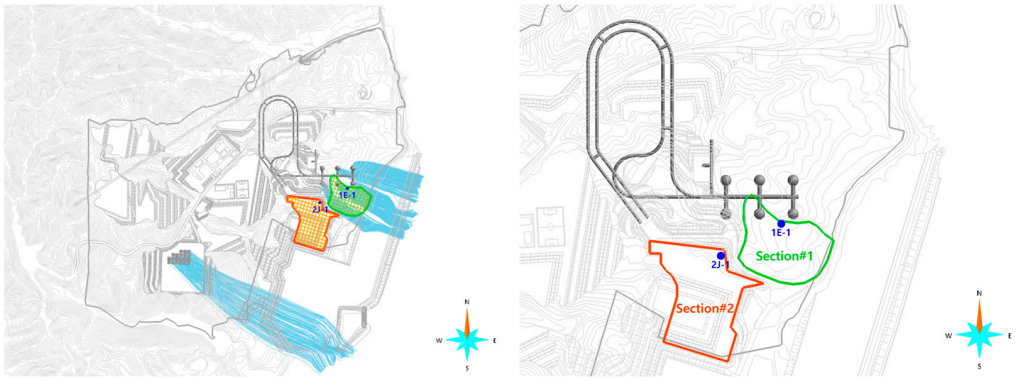
Well	Mean Groundwater Darcy Velocities (m/day)						
	SILO #1	SILO #2	SILO #3	SILO #4	SILO #5	SILO #6	Mean
2I-1	1.15×10^{-3}	-	-	-	-	-	1.15×10^{-3}
2J-1	1.42×10^{-3}	-	-	-	-	-	1.42×10^{-3}
2K-1	8.31×10^{-4}	-	-	-	-	-	8.31×10^{-4}

For Section #2, where particle influx to wells originated solely from Silo #1, the radionuclide inventory remained constant and transport was influenced only by groundwater flow characteristics. Therefore, dose assessment was not required for the selection of the representative well location.

Among the three locations showing complete particle influx, location 2J-1 demonstrated both the shortest mean contaminant transport distance via groundwater and the highest Darcy velocity. Based on these hydrogeological characteristics, location 2J-1 was designated as the representative well location for Section #2.

4.3. Groundwater Flow Changes with Pumping Rates

Figure 18 illustrates representative wells from two distinct sections, and further shows that the analysis demonstrates how pumping rates affect groundwater flow dynamics at these potential locations.



(**a**) (**b**)

Figure 18. Representative well locations considering groundwater flow patterns: (**a**) site overview; (**b**) detailed view of silo area.

The selection of representative wells was guided by the performance of engineered and natural barriers within the multi-barrier system. In Section #1, location 1E-1 was selected based on hydrogeological parameters and radiological impacts, particularly influenced by Silo #5, where cellulose-containing waste enhances radionuclide mobility through the engineered barrier system. In Section #2, location 2J-1 was chosen for its hydrogeological characteristics, including particle influx ratios, groundwater Darcy velocities, and contaminant transport distances, as this area was influenced by Silo #1, providing predictable migration pathways through the natural barrier.

4.3.1. Sensitivity Analysis Results of Pumping Rates at Section #1

To evaluate the groundwater impacts of well pumping, assessments were conducted by varying pumping rates up to 50,000 m^3/year, focusing on the relationship between pumping rates and particle inflow ratios at the representative well location 1E-1 in Section #1, as illustrated in Figure 19a. The results indicated no particle inflow from Silo #6 and demonstrating a typical pattern of increasing particle inflow with higher pumping rates.

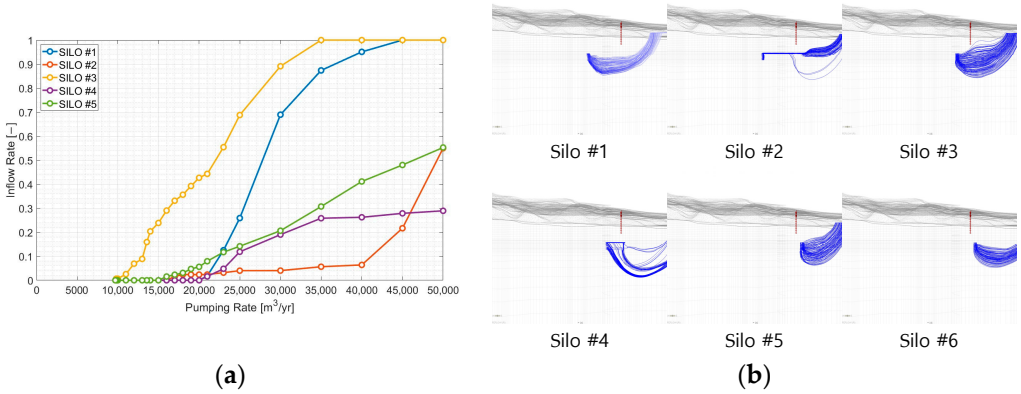


Figure 19. Contaminant transport analysis at representative well (1E-1) in Section #1 under varying pumping rates: (**a**) correlation between pumping rates and particle inflow ratios; (**b**) groundwater flow patterns around the well at the pumping rate where particle inflow ceases.

Particle influx began at different pumping rate thresholds: 21,000 m^3/year for Silo #1, 17,000 m^3/year for Silo #2, 9800 m^3/year for Silo #3, 16,000 m^3/year for Silo #4, and 21,000 m^3/year for Silo #5. Silos #1 and #3, which intersect the primary flow path, showed 100% particle influx at pumping rates exceeding 45,000 m^3/year. Silos #2 and #4, located upstream of the hypothetical well and creating reverse flows, demonstrated relatively lower influence. Silo #5, although positioned opposite to the dominant advective flow but in proximity, exhibited a clear trend of increasing particle influx with higher pumping rates.

At a pumping rate threshold of 9700 m^3/year, detailed analysis revealed no particle inflow from any silo. As shown in Figure 19b, Silo #6 maintained its original groundwater flow patterns without significant alterations. In contrast, Silo #3, located very close to the hypothetical well and along the primary groundwater flow path, exhibited the smallest variation in travel distance. For Silo #2, as the pumping rate increased, particles initially moving toward the ocean reversed their direction and flowed back into the well, resulting in increased travel distances. This suggests that, depending on the surrounding environment, deviations from typical groundwater flow patterns can occur.

The relationship between pumping rates and contaminant transport distances, as shown in Figure 20a, demonstrates an inverse correlation, with transport distances generally decreasing as pumping rates increase. However, spatial heterogeneity in hydrogeological conditions leads to varying responses across different zones. Silo #3, located closest to the hypothetical well, exhibits minimal variation in transport distances. In contrast, Silo #2

shows a positive correlation between pumping rates and transport distances, due to the redirection of particles from their initial ocean-bound trajectory toward the well. Figure 20b illustrates the spatial distribution of contaminant migration patterns from each silo under various pumping rate scenarios.

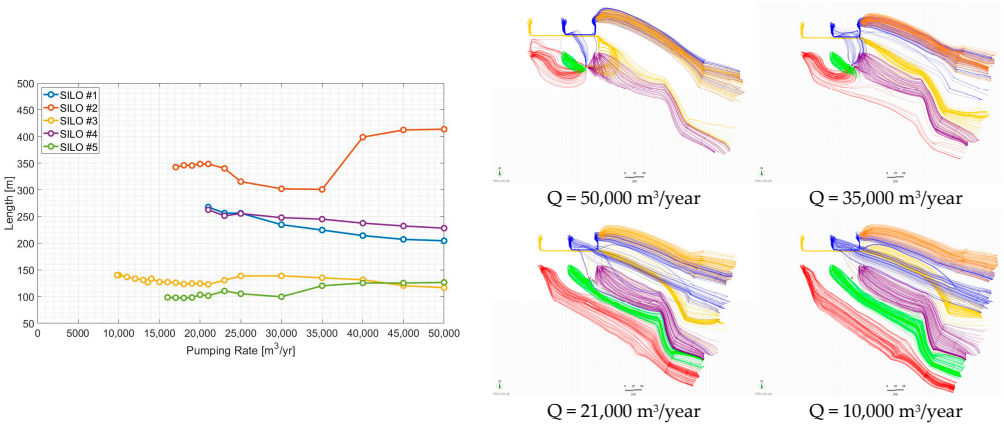


Figure 20. Contaminant transport analysis at representative well (1E-1) in Section #1 under varying pumping rates: (**a**) relationship between pumping rates and contaminant transport distances; (**b**) contaminant pathways under varying pumping rates.

The relationship between pumping rates and Darcy velocities, as depicted in Figure 21a, shows a modest positive correlation, despite relatively small variations in magnitude. Spatial heterogeneities in the hydraulic conductivity field result in localized deviations from this general trend, particularly in areas with discontinuities or enhanced permeability. Figure 21b illustrates that varying pumping rates create distinct zones of influence around the extraction well, leading to modifications in the hydraulic gradient. These changes in the hydraulic gradient, in turn, affect the geometry of flow paths and their associated flow velocities.

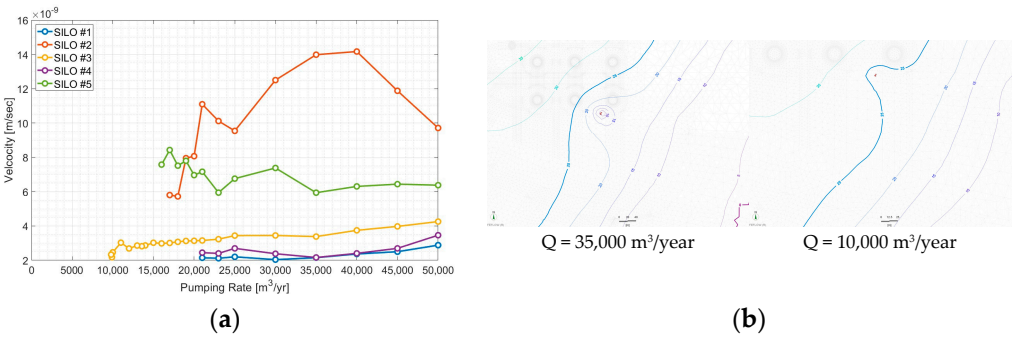


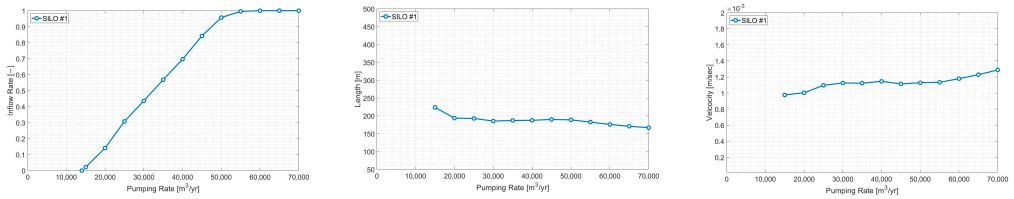
Figure 21. Contaminant transport analysis at representative well (1E-1) in Section #1 under varying pumping rates: (**a**) relationship between pumping rates and Darcy velocities; (**b**) spatial distribution of hydraulic-heads under different pumping conditions.

4.3.2. Sensitivity Analysis Results of Pumping Rates at Section #2

To assess the impact of varying pumping rates on particle inflow ratios, contaminant transport distances, and Darcy velocities at representative well 2J-1 in Section #2, a series of simulations were conducted with pumping rates up to 70,000 m^3/year. Due to the well's upstream location relative to the groundwater flow direction, no particle influx was observed from Silos #2 through #5, even at maximum pumping rates.

The analysis of pumping rates and particle influx ratios, as depicted in Figure 22a, indicates that particle influx from Silo #1 commences at a threshold of 15,000 m^3/year,

with capture efficiency nearing saturation beyond 60,000 m^3/year. Figure 22b illustrates an inverse relationship between pumping rates and contaminant transport distances, generally showing a decrease in transport distances at higher pumping rates, though local hydrogeological heterogeneities introduce some variability. Additionally, Figure 22c demonstrates a slight positive correlation between pumping rates and Darcy velocities; however, the magnitude of these velocity changes remains relatively modest.



(**a**) (**b**) (**c**)

Figure 22. Contaminant transport analysis at representative well (1E-1) in Section #1 under varying pumping rates: (**a**) correlation between pumping rates and particle inflow ratios; (**b**) relationship between pumping rates and contaminant transport distances; (**c**) relationship between pumping rates and Darcy velocities.

4.4. Radiological Impact Assessment Results

The analysis of radionuclide flux patterns in response to variable pumping rates demonstrated distinct spatial behaviors (Figure 23). In the near-field zone, radionuclide flux exhibited relative stability, primarily attributed to consistent groundwater flow characteristics. However, the far-field region displayed pronounced flux variations correlated with pumping-induced modifications in groundwater flow dynamics. The representative wells in Sections #1 and #2 revealed that carbon-14 (^{14}C) dominated the near-field region, primarily due to its high initial inventory. In contrast, technetium-99 (^{99}Tc) demonstrated preferential transport in the far-field region, closely correlating with groundwater flow patterns due to its anionic nature and minimal sorption interactions with the surrounding porous media. These observations emphasize the critical role of initial radionuclide inventory and geochemical sorption properties in shaping the spatial distribution of contaminants within the groundwater system.

The analysis of pumping rate variations at the Section #1 representative well location demonstrates an inverse correlation with the dose conversion factor (DCF), as illustrated in Figure 24a. The resulting dose, calculated as the product of far-field flux and DCF, exhibits a complex response to pumping rate variations. The dose increases with higher pumping rates due to the dominant influence of far-field flux, as illustrated in Figure 24b. Among the analyzed radionuclides, niobium-94 (^{94}Nb) exhibited the highest dose conversion factor (DCF) and emerged as the dominant dose contributor. Its enhanced mobility was attributed to the presence of cellulose-containing waste, which, under high-alkaline conditions, promotes the formation of ISA, reducing radionuclide sorption and increasing migration potential.

The analysis of pumping rate variations at the Section #2 representative well location also demonstrates an inverse correlation with the dose conversion factor (DCF), as illustrated in Figure 25a. Initially, the dose increases with higher pumping rates due to the dominant influence of far-field flux. However, as pumping rates continue to increase, the dose subsequently decreases due to the predominant effect of declining DCF values, as illustrated in Figure 25b. This non-linear relationship reflects the competing influences of flux enhancement and DCF reduction at elevated pumping rates. The analysis showed that radionuclide inflow to the well was limited to Silo #1. While ^{94}Nb exhibited the highest dose conversion factor (DCF), ^{99}Tc emerged as the dominant contributor to the total dose. This dominance is attributed to ^{99}Tc's substantially higher far-field flux values,

which outweighed the differences in DCF values between the radionuclides. The total dose calculations, determined by the product of DCF and far-field flux, identified ^{99}Tc as the most significant contributor despite its lower DCF compared to ^{94}Nb.

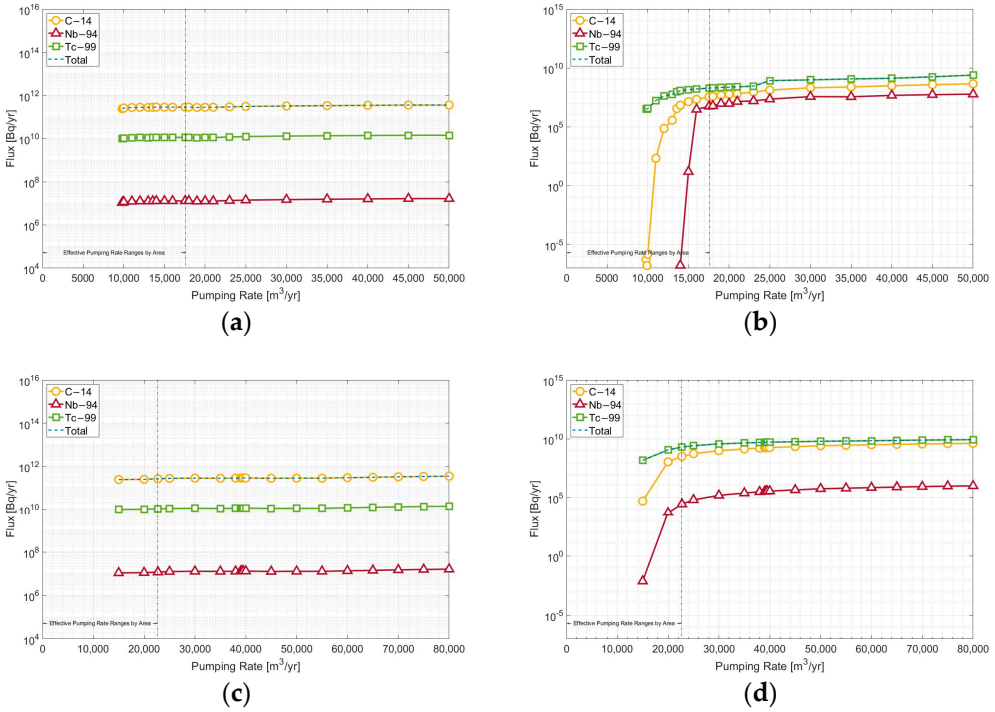


Figure 23. Variations in near-field and far-field flux with respect to changes in pumping rates: (**a**) near-field flux at Section #1 (1E-1); (**b**) far-field flux at Section #1 (1E-1); (**c**) near-field flux at Section #2 (2J-1); (**d**) far-field flux at Section #2 (2J-1).

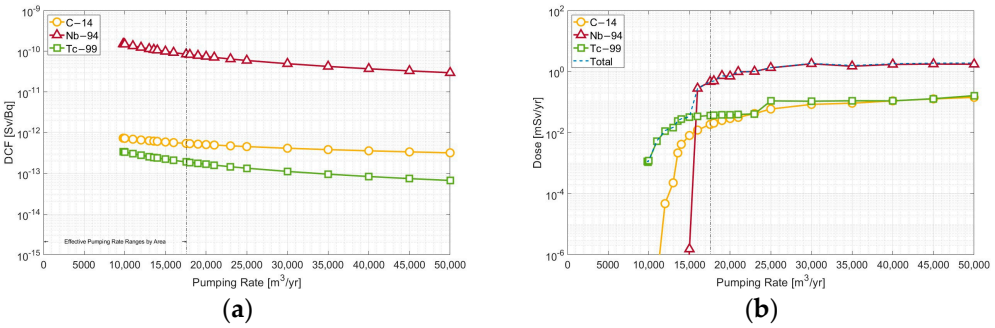
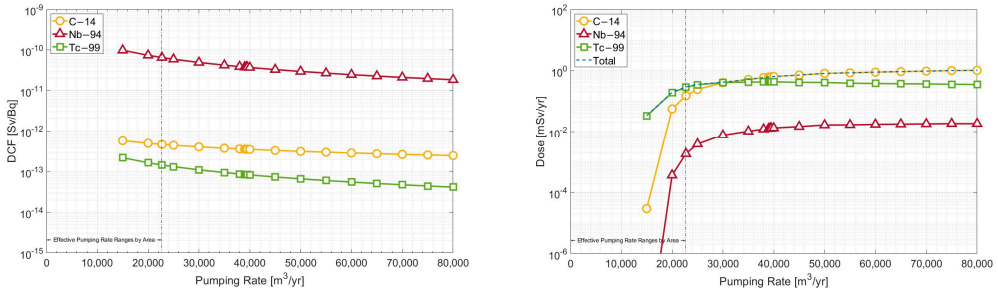


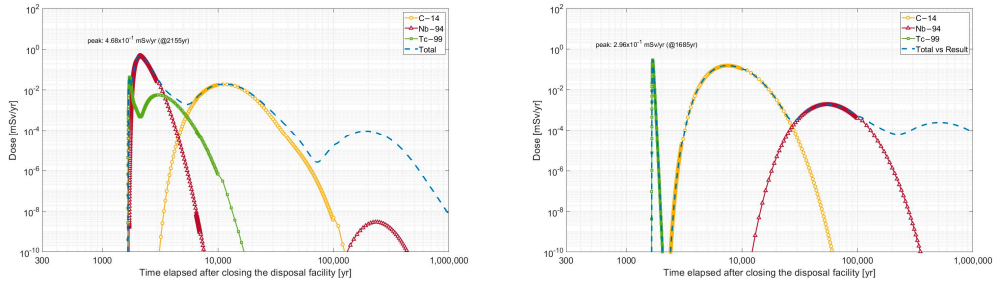
Figure 24. Variations in DCF and dose with respect to changes in pumping rates in Section #1: (**a**) DCF at Section #1 (1E-1); (**b**) dose at Section #1 (1E-1).

The dose evaluation results for the representative agro-livestock group farming the maximum area in each region are presented in Figure 26. At representative well 1E-1 in Section #1, the maximum exposure dose is 4.68 $\times$ 10^{-1} mSv/year, occurring 2115 years after the closure of the disposal facility (Figure 26a). The required pumping volume for the 37,689 m^2 area is 17,543 m^3/year, with contaminants originating from Silos #2, #3, and #5. The dominant radionuclide contributing to the dose is ^{94}Nb, primarily associated with the disposal of cellulose-containing waste in Silo #5.



(**a**) (**b**)

Figure 25. Variations in DCF and dose with respect to changes in pumping rates in Section #2: (**a**) DCF at Section #2 (2J-1); (**b**) dose at Section #2 (2J-1).



(**a**) (**b**)

Figure 26. Dose evaluation results at representative locations: (**a**) representative well in Section #1 (1E-1); (**b**) representative well in Section #2 (2J-1).

The maximum exposure dose at representative well 2J-1 in Section #2 is evaluated at 2.96×10^{-1} mSv/year, occurring 1685 years after the closure of the disposal facility (Figure 26b). The required pumping volume for the 48,818 m^2 area is 22,723 m^3/year, with contaminants originating exclusively from Silo #1. Due to the relatively low disposal quantity of cellulose-containing waste, ^{94}Nb had a less significant impact compared to well 1E-1. The dominant radionuclide contributing to the dose is ^{99}Tc, a representative anionic radionuclide with low adsorption in the surrounding medium.

5. Conclusions

Through scenario screening and particle tracking analysis, the representative wells 1E-1 (Figure 15b) in Section #1 and 2J-1 (Figure 16b) in Section #2 were selected by comprehensively considering contaminant influx ratios, transport distances and velocities along groundwater pathways, radionuclide inventory, and potential land use. Radiological impact assessments showed that the intrusion doses at wells 1E-1 and 2J-1 were 4.68×10^{-1} mSv/year and 2.96×10^{-1} mSv/year, respectively, both of them remain within the regulatory limit of 1 mSv/year. During the initial licensing stage, the safety assessment was conducted under overly simple assumptions without considering site-specific characteristics, resulting in an estimated dose of up to 9.50×10^{-1} mSv/year [27]. These simple assumptions not only produced overestimated doses but also revealed the difficulty of ensuring safety while efficiently operating the facility within a limited space. In contrast, the reassessment, which incorporated site-specific characteristics, demonstrated the facility's safety with an additional safety margin.

The analysis reveals that radionuclide transport and dose contributions are primarily governed by local hydrogeological conditions, often overriding theoretical dose conversion factor (DCF) values. This highlights the necessity of:

- Comprehensive hydrogeological characterization,
- A detailed understanding of radionuclide transport mechanisms, and

- The implementation of precise and targeted monitoring systems.

Overall, this study provides valuable insights for enhancing safety assessment frameworks for radioactive waste disposal facilities. By integrating site-specific characteristics, these frameworks can optimize safety strategies, ensuring long-term radiological safety through evidence-based decision making.

Author Contributions: Conceptualization, C.-M.L. and S.-G.K.; methodology, S.-G.K., H.-I.K. and J.-S.Y.; software, S.-G.K. and H.-I.K.; analysis, S.-G.K., H.-I.K. and J.-S.Y.; investigation, S.-G.K., J.-S.Y., C.-H.K. and H.H.; resources, C.-M.L., data curation, S.-G.K., J.-S.Y., C.-H.K. and H.H.; writing—original draft preparation, S.-G.K. and H.-I.K.; writing—review and editing, J.-S.Y. and C.-H.K.; visualization, S.-G.K., H.-I.K. and H.H.; supervision, C.-M.L. All authors have read and agreed to the published version of the manuscript.

Funding: This work was supported by the Korea Institute of Energy Technology Evaluation and Planning (KETEP) grant funded by the Korea government Ministry of Trade, Industry and Energy (Project Number: RS-2023-00236697) and the Global—Learning & Academic research institution for Master's·PhD students, and Postdocs (LAMP) Program of the National Research Foundation of Korea (NRF) grant funded by the Ministry of Education (No. RS-2023-00301938).

Data Availability Statement: The data presented in this study are available on request from the corresponding author.

Acknowledgments: The authors appreciate the support from Korea Radioactive Waste Agency.

Conflicts of Interest: The authors declare no competing interests. The author Jeoung-Seok Yoon was employed by the company DynaFrax UG Ltd. There is no conflict of interest between any of the authors and the company DynaFrax UG Ltd. The author Chan-Hong Kim was employed by the company Korea Mine Rehabilitation and Mineral Resources Corporation (KOMIR). There is no conflict of interest between any of the authors and the company Korea Mine Rehabilitation and Mineral Resources Corporation (KOMIR).

References

1. Wu, J.; Fu, Q.; Sial, M.S.; Pavel, C.D.; Samad, S.; Matac, L.M. Causal Relationship between Nuclear Energy, Carbon-Dioxide Emission and Economic Growth: Empirical Evidence from China. *Front. Energy Res.* **2022**, *10*, 993818. [CrossRef]
2. Krūmiņš, J.; Kļaviņš, M. Investigating the Potential of Nuclear Energy in Achieving a Carbon-Free Energy Future. *Energies* **2023**, *16*, 3612. [CrossRef]
3. World Nuclear Association. *International Nuclear Waste Disposal Concepts*; WNA: London, UK, 2023.
4. IAEA. *Scientific and Technical Basis for Geological Disposal of Radioactive Wastes*; Technical Reports Series No. 413; IAEA: Vienna, Austria, 2003.
5. IAEA. *Disposal of Radioactive Waste*; IAEA Safety Standards Series No. SSR-5; IAEA: Vienna, Austria, 2011.
6. U.S. Department of Energy. *Pioneering Nuclear Waste Disposal*; DOE: Carlsbad, NM, USA, 2000.
7. IAEA. *Migration and Biological Transfer of Radionuclides from Shallow Land Burial*; Technical Report Series No. 579; IAEA: Vienna, Austria, 1990.
8. Di Dato, M.; Fiori, A.; de Barros, F.P.J.; Bellin, A. Radial solute transport in highly heterogeneous aquifers: Modeling and experimental comparison. *Water Resour. Res.* **2017**, *53*, 5725–5741. [CrossRef]
9. Cheong, J.-Y.; Hamm, S.-Y.; Lim, D.-H.; Kim, S.-G. Hydraulic Parameter Generation Technique Using a Discrete Fracture Network with Bedrock Heterogeneity in Korea. *Water* **2017**, *9*, 937. [CrossRef]
10. IAEA. *The Safety Case and Safety Assessment for the Disposal of Radioactive Waste*; Specific Safety Guide No. SSG-23; IAEA: Vienna, Austria, 2012.
11. Nuclear Energy Agency. *Engineered Barrier Systems and the Safety of Deep Geological Repositories*; NEA No. 3615; OECD: Paris, France, 2003.
12. IAEA. *Human Intrusion in the Context of Disposal of Radioactive Waste*; IAEA-HIDRA; IAEA: Vienna, Austria, 2015.
13. Nuclear Safety and Security Commission of the Republic of Korea. *Radiological Protection Criteria for Low and Intermediate Level Radioactive Waste Disposal Facility*; NSSC Notice No. 2017-62; NSSC: Seoul, Republic of Korea, 2017.
14. IAEA. *Safety Assessment Methodologies for Near Surface Disposal Facilities*; IAEA-ISAM-1; IAEA: Vienna, Austria, 2004.

15. Hong, S.W.; Park, S.; Park, J.B. Safety Assessment on the Human Intrusion Scenarios of Near Surface Disposal Facility for Low and Very Low Level Radioactive Waste. *J. Nucl. Fuel Cycle Waste Technol.* **2016**, *14*, 79–90. [CrossRef]
16. KORAD (Korea Radioactive Waste Agency). Wolsong Low and Intermediate Level Radioactive Waste Disposal Center. 2024. Available online: https://www.korad.or.kr/korad-eng/html.do?menu_idx=37 (accessed on 18 September 2024).
17. Korea Hydro & Nuclear Power Co., Ltd. *Radiological Environmental Impact Assessment Report for Shin-Wolsong Units 1 & 2 (Section 2.2.1 Land Use Status)*; KHNP: Gyeongju, Republic of Korea, 2011.
18. National Geographic Information Institute. *National Atlas of Korea*; NGII: Suwon, Republic of Korea, 2020.
19. Korea Meteorological Administration. *Climate Characteristics of Korea*; KMA: Seoul, Republic of Korea, 2023.
20. World Meteorological Organization. *Guidelines on the Calculation of Climate Normals*; WMO-No. 1203; WMO: Geneva, Switzerland, 2017.
21. Korea Radioactive Waste Agency. *Safety Analysis Report for the First Phase LILW Disposal Facility*; KORAD: Gyeongju, Republic of Korea, 2007.
22. Korea Hydro & Nuclear Power Co., Ltd. *Radiological Environmental Impact Assessment Report for Low and Intermediate Level Radioactive Waste Disposal Facility*; KHNP: Gyeongju, Republic of Korea, 2006.
23. Guo, Z.; Ma, R.; Zhang, Y.; Zheng, C. Contaminant transport in heterogeneous aquifers: A critical review of mechanisms and numerical methods of non-Fickian dispersion. *Sci. China Earth Sci.* **2021**, *64*, 1224–1241. [CrossRef]
24. International Commission on Radiological Protection. *Radiation Protection Recommendations as Applied to the Disposal of Long-Lived Solid Radioactive Waste*; ICRP Publication 81; Ann. ICRP 28(4); ICRP: Ottawa, ON, Canada, 1998.
25. Su, X.; Befus, K.M.; Hummel, M.A. Shoreline barriers may amplify coastal groundwater hazards with sea-level rise. *Sci. Rep.* **2024**, *14*, 15559. [CrossRef] [PubMed]
26. Van Loon, L.R.; Glaus, M.A. Review of the Kinetics of Alkaline Degradation of Cellulose in View of its Relevance for Safety Assessment of Radioactive Waste Repositories. *J. Environ. Polym. Degr.* **1997**, *5*, 97–109. [CrossRef]
27. KHNP. *Safety Analysis Report for Phase 1 Low- and Intermediate-Level Radioactive Waste Disposal Facility (SAR)*; Korea Hydro & Nuclear Power Co., Ltd.: Seoul, Republic of Korea, 2008. (In Korean)

Disclaimer/Publisher's Note: The statements, opinions and data contained in all publications are solely those of the individual author(s) and contributor(s) and not of MDPI and/or the editor(s). MDPI and/or the editor(s) disclaim responsibility for any injury to people or property resulting from any ideas, methods, instructions or products referred to in the content.

Reproduced with permission of copyright owner. Further reproduction prohibited without permission.